A REDUCED ORDER MODEL FOR OPTIMAL CENTRIFUGAL PUMP DESIGN

Luca d'Agostino[1,2♦], Angelo Pasini[1*], Dario Valentini[2♠], Giovanni Pace[1♣], Lucio Torre[1♥] and Angelo Cervone[1♣]

[1]ALTA S.p.A.
5 Via Gherardesca, Ospedaletto, Pisa, 56121, Italy
*a.pasini@alta-space.com ♣g.pace@alta-space.com ♥l.torre@alta-space.com ♣a.cervone@alta-space.com

[2]University of Pisa, Aerospace Engineering Department
12 Via G. Caruso, Pisa, 56126, Italy
♠dariovalentini83@gmail.com ♦luca.dagostino@ing.unipi.it

Abstract

A reduced order model for preliminary design and noncavitating performance prediction of radial turbopumps has been illustrated in a previous paper presented by the same authors. The model expresses the 3D incompressible, inviscid, irrotational flow through helical blades with slow axial variations of the pitch and backsweep by superposing a 2D cross-sectional axial vorticity correction to a fully-guided flow with axisymmetric stagnation velocity in the meridional plane. Application of the relevant governing equations yields a set of constraints for the axial evolution of the blade pitch and backsweep that allows for the closed form definition of the impeller geometry and flowfield in terms of a reduced number of controlling parameters. In turn, mass and momentum conservation are used to account for the mixing of the flow leaving the impeller and its coupling with 2D reduced order models of the flow in the diffuser (if any) and the volute, thus generating the information necessary for completing the geometric definition of the machine and for determining its ideal noncavitating performance in accordance with the resulting flowfield.
In the present paper, the above ideal flow model has been interfaced with the calculation of boundary layers inside the blade channels and other major forms of flow losses, with the aim of developing an effective tool for rapid parametric optimization of the machine geometry and performance under appropriate design constraints such as target values of the specific speed, flow coefficient and impeller blading solidity.

Nomenclature

b_B	=	blade tip thickness
b_{I2}	=	impeller discharge blade width
B	=	Blockage
K	=	PDE costant
N	=	number of blades
f	=	friction factor
p , p_t	=	static and total pressures
P	=	blade axial pitch
r	=	radial coordinate, radius
Re	=	Reynolds number
s	=	space between two consecutive blades developed over a cylindrical surface
$\boldsymbol{u}$	=	flow velocity
u	=	radial flow velocity
v	=	azimuthal flow velocity
v^*	=	wall friction velocity
$\dot{V}$	=	volumetric flow rate
w	=	axial flow velocity
x	=	curvilinear streamline coordinate
y	=	orthogonal curvilinear streamline coordinate
z	=	axial coordinate
α	=	turning angle
β_B	=	blade taper azimuthal half-angle
δ	=	BL thickness
δ_2°	=	impeller discharge deviation angle
δ^*	=	BL displacement thickness
γ	=	blade angle from axial direction
λ	=	streamline angle from merdidional plane
ϑ	=	azimuthal coordinate
θ	=	BL momentum thickness
ϑ_{Bk}	=	azimuthal coordinate on the k-th blade surface
ρ	=	flow density
σ	=	solidity $\sigma = \int \frac{dc}{s}$
τ_w	=	wall shear stress
Φ	=	flow coefficient
Φ_2	=	flow coefficient referred to impeller discharge section: $\Phi_2 = \dot{V} / (2\pi r_2 b_{I2} \Omega r_2)$
χ	=	backsweep angle from radial direction
ψ	=	velocity stream function
Ψ	=	total head coefficient
Ω	=	impeller rotational speed

Superscripts

q'	=	value of q in the rotating frame
$\overline{q}$	=	mean value of q

q^+ = BL inner adimensional variable
s = slip azimuthal velocity
$\hat{\boldsymbol{u}}$ = fully-guided flow
$\tilde{\boldsymbol{u}}$ = slip flow

Subscripts

bs = backswept blade
BL = boundary layer
B = blocked
ch = blade channel
eq = equivalent duct
D = diffuser, design conditions
des = design conditions
E = Euler pressure rise
F = friction
M = mescolation
I = impeller
H = hub radius
ss = suction side
ps = pressure side
s = slip
st = stagnation plane
T = tip radius
0 = upstream station
1 = impeller inlet station (1)
2 = impeller outlet station (2)
3 = diffuser outlet station (3)
4 = volute outlet section station (4)
5 = pump discharge station (5)

Acronyms

BL = boundary layer
ODE = ordinary differential equation
2D = two-dimensional
3D = three-dimensional

Introduction

Where high total thrust impulses are needed and high pressures are used in the combustion chamber turbopump feed systems represent the best solution for liquid propellant rocket engines. Centrifugal pumps are universally recognized as the most suitable solution for pumping propellants in large rocket units. However, their simplicity, high reliability, light weight, wide operating range, relatively low development time and cost make centrifugal pumps widely used also for an almost endless variety of engineering applications.

Severe limitations are associated with the design of high power density, dynamically stable machines capable of meeting the extremely demanding pumping, suction and reliability requirements of space transportation systems (Stripling et al., [1]). Current rocket propellant feed turbopumps often employ an inducer upstream of the centrifugal stage in order to avoid unacceptable cavitation, improve the suction performance and reduce the propellant tank pressure and weight. Radial turbopumps usually have a smaller number of blades (typically about eight) than compressors, as they require thicker blades in order to sustain the higher bending loads generated by liquids, and therefore comparatively generate more flow blockage (Brennen, [2]).

Typical iterative schemes (Laskshminarayana, [3]) for the design of the blading and flow path in centrifugal machines involve a preliminary step in which the main dimensions of the impeller and the diffuser are determined. Then, a first approximation of the geometry of these components is generated and a relatively elaborate optimization process is carried out with the objective of attaining maximum efficiency. Recently numerical optimization strategies based on the Redial Basis Neural Network (RBNN) have been applied by many researches (Huppertz et al. [4], Kim et al. [5], Choi et al. [6], Rai et al. [7], Kim et al. [8]). Other systematic numerical optimization approaches are based on the mean streamline analysis (Oh et al., [9]), the three-dimensional inverse method coupled with optimization algorithm (Ashihara et al., [10]) and the numerical flow analysis (Visser et al., [11]).

In this context, therefore, the development of 3D theoretical models capable of rapidly predicting the geometry and performance of radial impellers in order to provide indications for the preliminary design of the machine is of particular interest to rocket engineers. However, not many such models have been proposed so far, probably due to the difficulty of adequately describing the 3D flowfield through the impeller blades. Therefore, designers often refer to simple "rules of thumb", or to the general indications of design manuals, such as the one published by NASA (Douglass, [12]).

A useful tool for the geometrical definition and the preliminary design of space rocket axial inducers is represented by the reduced order model developed at ALTA S.p.A. (d'Agostino et al., [13]). In particular, the model has been successfully used for designing and manufacturing two inducers (a 3-bladed and a 4-bladed one) that have been tested in the framework of an ESA funded activity (Torre et al. [14], Cervone et al. [15], Pasini et al. [16]). The natural extension of this approach under more general assumptions has allowed for the development of a new analytical model suitable for application to centrifugal pumps with helical blades with slow axial changes of the pitch and backsweep angles. The ideal flow version of the model and its potential for application to the preliminary design and performance prediction of radial turbopumps have been briefly illustrated in an earlier publication (d'Agostino et al., [17]). The present paper reports the evolution of that model with the introduction of viscous effects and other main sources of flow losses and its potential for application to the efficient setting and solution of an optimization problem aimed at determining the optimal values for the turbopump's geometrical parameters under appropriate design constraints, such as assigned values of the specific speed, flow rate and blading solidity.

Inviscid Preliminary Design and Performance Prediction

Following the same approach illustrated in d'Agostino et al., [17], the model expresses the 3D incompressible, inviscid, irrotational flow through helical blades with slow axial variations of the pitch and backsweep by superposing a 2D cross-sectional axial vorticity correction with velocity $\tilde{\boldsymbol{u}}$ to a fully-guided flowfield $\hat{\boldsymbol{u}}$ with axisymmetric stagnation velocity in the meridional plane.

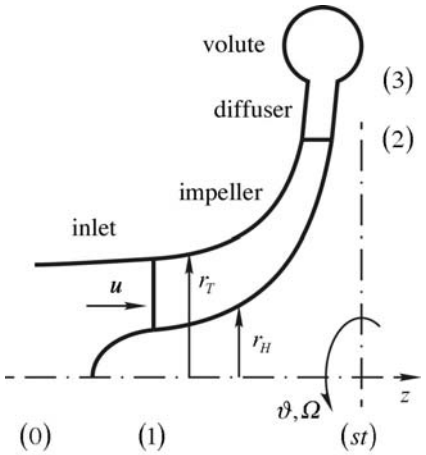

Fig.1 Radial machine schematic and nomenclature.

Application of the relevant governing equations yields a set of constraints for the axial evolution of the blade pitch and backsweep that allows for the closed form definition of the impeller geometry and flowfield in terms of a reduced number of controlling parameters. In particular, once the location of the stagnation plane, z_{st}, has been fixed, the tip and hub radius profiles in the meridional plane up to the exit radius, r_2, are defined by the stagnation flow streamlines through the inlet tip and hub radii, r_{T1} and r_{H1}. Finally, in the stated assumptions only the tip inlet blade angle, γ_{T1}, has to be assigned in order to complete the geometric definition of the impeller blades.

In turn, mass and momentum conservation are used to account for the mixing of the flow leaving the impeller and its coupling with 2D reduced order models of the flow in the diffuser and the volute. In these latter models, the information necessary for completing the geometric definition of the machine only consists in a set of three parameters: the diffuser width, b_D, its outer diameter, r_3, and the design flow coefficient expressed in terms of the inlet tip incidence angle, i_{T1}:

$$\Phi = \frac{\pi\left(1-r_{H1}^2/r_{T1}^2\right)r_{T1}^3/r_2^3}{\tan\left(\gamma_{T1}+i_{T1}\right)}$$

The ideal noncavitating performance can be computed from the resulting flowfield by means of Euler's equation as follows:

$$\Psi = \frac{\Delta p_t}{\rho\Omega^2 r_2^2} = \frac{\rho\Omega r_2 \overline{v}_2}{\rho\Omega^2 r_2^2} = \frac{\overline{v}_2}{\Omega r_2}$$

where:

$$\overline{v}_2 \simeq \overline{\hat{v}}_2 + \overline{v}_S$$

is the axially-averaged azimuthal velocity at the impeller discharge, which comprises the averaged values of the fully-guided velocity, $\hat{v}_2$, and of the vorticity correction, $\overline{v}_S$, at the impeller discharge.

For helical backswept blades the azimuthal velocity component of the fully-guided flow is expressed by:

$$\hat{v}(r,z) = \Omega r - \hat{w}(z)\tan\gamma(r,z) - \hat{u}(r)\tan\chi(z)$$

where the fully-guided axial, $\hat{w}$, and radial, $\hat{u}$, velocities are expressed by the components of the axisymmetric stagnation flowfield:

$$\hat{w}(z) = \hat{w}_1\frac{z-z_{st}}{z_1-z_{st}};\ \hat{u}(r) = -\frac{1}{2}r\frac{\hat{w}_1}{z_1-z_{st}}$$

and the angle γ, measured from the axial direction, includes both the effect of the axial variations of the helical pitch P_h of the blades and of their backsweep angle χ.

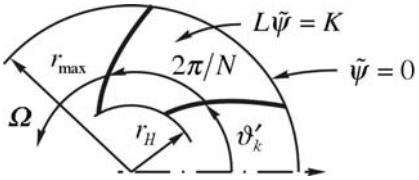

Fig.2 Blade channel cross-section.

The mass-averaged slip velocity along the azimuthal direction at rotor discharge, v_S, can be computed from the solution of the Poisson's boundary value problem for the stream function $\tilde{\psi}(r',\vartheta')$ of the slip flow on each axial cross-section of the blade channels (see Fig. 2) as follows (d'Agostino et al., [17]):

$$v_S(z) = \sum_{m=1}^{+\infty}\sum_{n=1}^{+\infty}\frac{\frac{K}{r_2\ln(r_2/r_H)}(-1)^m\left[1-(-1)^m\frac{r_2^2}{r_H^2}\right]\left(n-\frac{1}{2}\right)^{-2}}{\left(1+\frac{m^2\pi^2}{\ln^2(r_2^2/r_H^2)}\right)\left[\pi^2+\frac{\left(n-\frac{1}{2}\right)^2N^2\ln^2(r_2/r_H)}{m^2\cos^2\chi}\right]}$$

where:

$$K = 2\Omega - 4\pi\frac{\hat{w}_1}{P_1} + \frac{d\hat{w}}{dz}\tan\chi_1$$

is constant at all axial stations.

Analysis of Hydraulic Losses and Efficiency

In our previous work, the pumping performance of the machine has been evaluated under ideal flow conditions neglecting all sources of energy dissipation, consistently with the inviscid assumption originally introduced to solve for the machine geometry and flowfield. Clearly, the major contributions to the losses (typically arising from flow incidence at the blade leading edges, viscous and secondary flow effects, and turbulent mixing) play a crucial role for realistic performance prediction and optimization of hydraulic turbomachinery, and will be discussed in details for each element of the machine in this section.

IMPELLER

In order to better approximate the actual pumping characteristic of noncavitating impellers the main sources of performance degradation (flow incidence, friction, blockage, deviation and turbulent mixing) have to be accounted for.

The assumptions of fully-guided flow at the inducer leading edge are not accurately satisfied in practice. Incidence losses due to the sudden change of the flow direction at the leading edge of the inducer blades are expressed in terms of a nondimensional equivalent length $\left(L_{eq}/D_{ch}\right)=\frac{\Delta\alpha[\deg]}{3}$, function of the turning angle, $\Delta\alpha$, evaluated on the mean streamline:

$$\Delta p_{tI1} = f_{ch}\left(\frac{L_{eq}}{D_{ch}}\right)\frac{1}{2}\rho V_1'^2$$

where the friction factor f_{ch} depends on the Reynolds number based on the hydraulic diameter D_{ch} of the blade channels and V_1' is the relative flow velocity at the mean inlet radius.

Due to viscous effects, the development of the boundary layer on the inner surface of the blade channels introduces friction losses, flow blockage and, in case of differential grow of the displacement thickness on the pressure and suction blade surfaces, deviation of the flow at the impeller discharge. Moreover, the effective flow cross-section is also influenced by the thickness of the blades.

In order to assess the influence of all of these aspects on the pumping performance in a way explicitly depending on the geometry of the impeller blading, as required for realistic optimization of the machine, the evolution of the boundary layer has been estimated along the four streamlines ending at the mid points of the blade channel sides at the impeller discharge, considered as representative of exit boundary layer effects on their corresponding surfaces.

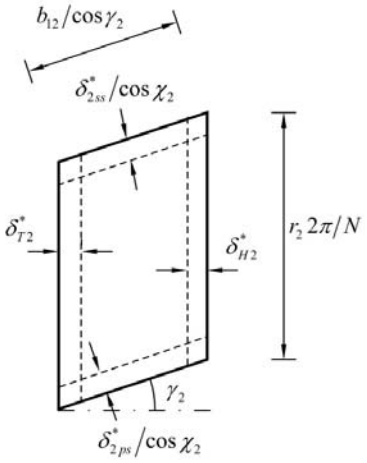

Fig.3 Approximate evaluation of the blockage at the impeller discharge section.

Consequently, the flow blockage at the impeller exhaust has been approximated by the following expression (see Fig. 3):

$$B_{BL2} \simeq \frac{\delta^*_{H2}\left(\frac{2\pi r_2}{N}-\frac{\delta^*_{2ss}}{\cos\chi_2}\right)+\delta^*_{T2}\left(\frac{2\pi r_2}{N}-\frac{\delta^*_{2ps}}{\cos\chi_2}\right)}{A_{ch}}+$$
$$+\frac{\frac{\delta^*_{2ss}\left(b_{I2}-\delta^*_{T2}\right)}{\cos\chi_2}+\frac{\delta^*_{2ps}\left(b_{I2}-\delta^*_{H2}\right)}{\cos\chi_2}}{A_{ch}}$$

where δ^*_{2ss}, δ^*_{2ps} and δ^*_{H2}, δ^*_{T2} are respectively the displacement BL thicknesses on the suction and pressure sides of the blades and on the impeller hub and tip, while b_{I2} is the exhaust axial blade height and A_{ch} is the nominal channel area.

Assuming tapered triangular blades, the additional flow blockage generated by the blade thickness at the impeller discharge (station 2 at $r=r_2$), is:

$$B_{B2} \simeq \frac{b_{I2}\left(b_{bT}+b_{I2}\tan\beta_b\right)}{A_{ch}}$$

where b_{bT} is the azimuthal tip blade thickness and β_b is the blade taper azimuthal half-angle.

Then the flow velocity at the impeller exit, corrected for blockage effects, is:

$$\boldsymbol{u}'_{2b}=\frac{\boldsymbol{u}'_2}{\left(1-B_2\right)} \quad\Rightarrow\quad \begin{cases} u'_{2b}=u'_2/\left(1-B_2\right) \\ v'_{2b}=v'_2/\left(1-B_2\right) \\ w'_{2b}=w'_2/\left(1-B_2\right) \end{cases}$$

where $B_2=B_{BL2}+B_{B2}$ is the total blockage at $r=r_2$.

The flow deviation at the impeller exhaust generated by the BL growth is:

$$\delta_2^\circ=\frac{\left(\left.\frac{d\delta^*_{ss}}{dx}\right|_2\sin\lambda_{ss2}-\left.\frac{d\delta^*_{ps}}{dx}\right|_2\sin\lambda_{ps2}\right)}{2}$$

where x is the curvilinear coordinate along the streamline and λ is the angle between the rotational axis and the streamline in the meridional plane. Consequently the resulting relative azimuthal velocity becomes:

$$v'_{2b\delta^\circ}=-u'_{2b}\tan\left[-\tan^{-1}\left(v'_{2b}/u'_{2b}\right)+\delta^\circ\right]$$

Finally, with the same approach used for the flow blockage, the total pressure loss at the impeller exhaust due to BL friction becomes:

$$\Delta p_{tBL2}\simeq\frac{\theta_{H2}}{A_{ch}}\left(\frac{2\pi r_2}{N}-\frac{\theta_{2ss}}{\cos\chi_2}\right)\frac{\rho U_{H2}^2}{2}+\frac{\theta_{T2}}{A_{ch}}\left(\frac{2\pi r_2}{N}-\frac{\theta_{2ps}}{\cos\chi_2}\right)\frac{\rho U_{T2}^2}{2}+$$
$$+\frac{\theta_{2ss}\left(b_{I2}-\theta_{T2}\right)}{A_{ch}\cos\chi_2}\frac{\rho U_{ss2}^2}{2}+\frac{\theta_{2ps}\left(b_{I2}-\theta_{H2}\right)}{A_{ch}\cos\chi_2}\frac{\rho U_{ps2}^2}{2}$$

where θ_{2ss}, θ_{2ps} and θ_{H2}, θ_{T2} are the momentum BL thicknesses on the suction and pressure sides of the blades and on the impeller hub and tip.

The evaluation of the evolution of the boundary layers along the above streamlines has been carried out in two steps: the preliminary identification of the streamline geometry, followed by the path integration of a suitable form of the parabolized boundary layer equations from the blade leading edge to the impeller discharge.

In general, the relative flow streamlines are defined in scalar terms by the coupled system of ODE's:

$$\begin{cases} \dfrac{dr}{ds} = \dfrac{u'}{\sqrt{u'^2+v'^2+w'^2}} & \text{with IC} \quad r(0)=r_0 \\ \dfrac{d\vartheta'}{ds} = \dfrac{v'}{r\sqrt{u'^2+v'^2+w'^2}} & \text{with IC} \quad \vartheta'(0)=\vartheta'_0 \\ \dfrac{dz}{ds} = \dfrac{w'}{\sqrt{u'^2+v'^2+w'^2}} & \text{with IC} \quad z(0)=z_0 \end{cases}$$

Exploiting the knowledge of the flowfield inside the rotor obtained as a result of the reduced order model, the above ODEs systems for the relative streamlines can be (numerically) integrated from the exhaust section to the inlet section with the ICs that corresponds to the mid points of the suction and pressure sides of the blades and of the impeller hub and shroud (Fig.4).

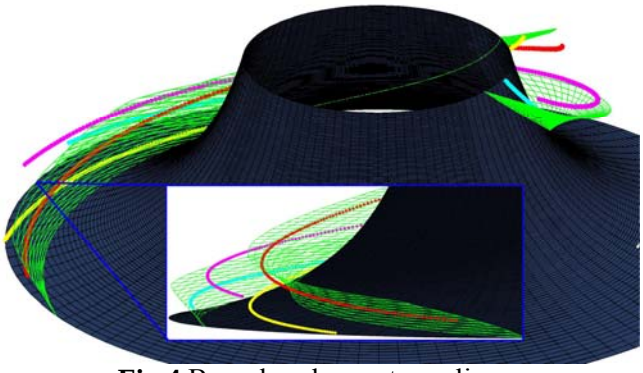

Fig.4 Boundary layer streamlines.

The governing equations for an incompressible axisymmetric laminar boundary layer on a surface rotating with angular speed Ω can be obtained from the laminar continuity and momentum equations in the relative frame:

$$\nabla \cdot \boldsymbol{u}' = 0$$

$$\boldsymbol{u}' \cdot \nabla \boldsymbol{u}' = -\frac{1}{\rho}\nabla p + \nu \nabla \cdot \left[\nabla \boldsymbol{u}' + (\nabla \boldsymbol{u}')^T \right] - 2\boldsymbol{\Omega} \times \boldsymbol{u}' + \Omega^2 \boldsymbol{r}$$

by writing the equations in the streamwise BL coordinates x, y, n (where $u_n = 0$) with the standard BL approximation ($\frac{v}{u} \sim \frac{\delta}{x} << 1$ and $\frac{\partial}{\partial y} \sim \frac{1}{\delta}$) and neglecting the Coriolis forces. Then:

$$\frac{\partial (r_0 u_x)}{\partial x} + r_0 \frac{\partial u_y}{\partial y} = 0$$

$$0 \simeq -\frac{1}{\rho}\frac{\partial p}{\partial y} + \Omega^2 r_0 \cos\lambda$$

$$u_y \frac{\partial u_x}{\partial y} + u_x \frac{\partial u_x}{\partial x} = -\frac{1}{\rho}\frac{\partial p}{\partial x} + \nu \frac{\partial^2 u_x}{\partial y^2} + \Omega^2 r \sin\lambda \cos\mu$$

where r_0 is the radial distance from the axis, λ is the meridional angle of the BL surface from the axial z direction and μ is the angle of the BL streamline from the meridional plane.

Moreover, by differentiating the steady Bernoulli's equation along a relative streamline:

$$-\frac{1}{\rho}\frac{\partial p}{\partial y} = -\Omega^2 r \frac{dr}{dy} \simeq -\Omega^2 r_0 \cos\lambda$$

$$-\frac{1}{\rho}\frac{\partial p}{\partial x} \simeq U\frac{dU}{dx} - \Omega^2 r \frac{dr_0}{dx} \simeq U\frac{dU}{dx} - \Omega^2 r_0 \sin\lambda \cos\mu$$

where U is the relative streamwise velocity of the free stream and, eliminating the pressure from the BL momentum equations, the following expressions can be obtained:

$$0 \simeq \Omega^2 r_0 \cos\lambda + \Omega^2 r_0 \cos\lambda$$

$$u_y \frac{\partial u_x}{\partial y} + u_x \frac{\partial u_x}{\partial x} = U\frac{dU}{dx} + \nu \frac{\partial^2 u_x}{\partial y^2}$$

The first equation is identically verified, while the second is independent on Ω since in the stated assumptions centrifugal effects in the boundary layer and in the freestream balance each other.

Finally, the turbulent axisymmetric BL equations on rotating surfaces can be obtained by standard Reynolds averaging in the form:

$$\frac{\partial (r_0 \bar{u}_x)}{\partial x} + \frac{\partial (r_0 \bar{u}_y)}{\partial y} = 0$$

$$\bar{u}_x \frac{\partial \bar{u}_x}{\partial x} + \bar{u}_y \frac{\partial \bar{u}_x}{\partial y} = U\frac{dU}{dx} + \frac{1}{\rho}\frac{\partial \tau_t}{\partial y}$$

where bars indicate the mean flow properties, primes the turbulent fluctuations and $\tau_t = \mu \frac{\partial \bar{u}_x}{\partial y} - \rho u'_x u'_y$ is the turbulent shear stress.

An approximate solution of these equations can then be obtained, for instance, by means of the inner variables method proposed by White [18].The basic idea of the method is that, when expressed in terms of the inner variables:

$$u^+ = \frac{\bar{u}_x}{v^*}, \quad v^+ = \frac{\bar{u}_y}{v^*}, \quad y^+ = \frac{y v^*}{\nu} \quad \text{with} \quad v^* = \sqrt{\frac{\tau_w}{\rho}}$$

the velocity profile inside the boundary layer can be approximated by the logarithmic law of the wall with a wake correction $w(y^+, \xi)$ function of y^+ and of a single dimensionless parameter $\xi(x)$:

$$u^+ = \frac{1}{\kappa}\ln y^+ + B + w\left[y^+, \xi(x)\right] \quad \text{with} \quad \begin{cases} B \simeq 5.5 \\ \kappa \simeq 0.4 \end{cases}$$

Here, following White [18], $w\left[y^+, \xi(x)\right] = 0.6\xi y^+$ where $\xi = \frac{\mu}{\tau_w v^*} U \frac{dU}{dx}$ is the pressure-gradient correlation parameter as defined by Mellor [19].

Introducing the inner variables formulation, eliminating $\bar{u}_y$ with the continuity equation, integrating the BL momentum relation with respect to y^+ from the wall ($y^+ = 0$, $\tau = \tau_w$) to the freestream $y^+ = \delta^+$ ($u^+ = U^+$, $\tau = 0$) and nondimensionalizing the results by means of the positions $x = 2r_2 x_*$ and $U = \Omega r_2 U_*$, the final ordinary differential equation for the skin friction parameter $\lambda = U^+$ can be written in normal form as:

$$\frac{d\lambda}{dx_*}=\frac{U_*\,\mathrm{Re}_D-\left(\lambda^2\delta^+-G\right)\lambda\frac{1}{U_*}\frac{dU_*}{dx_*}+\frac{\lambda^4 H}{\mathrm{Re}_D}\frac{d^2}{dx_*^2}\left(\frac{1}{U_*}\right)-K\lambda\frac{1}{r_0}\frac{dr_0}{dx_*}}{G-\frac{3\lambda^3 H}{\mathrm{Re}_D}\frac{d}{dx_*}\left(\frac{1}{U_*}\right)}$$

Here $\mathrm{Re}_D=\frac{2\Omega r_2^2}{\nu}$ is the Reynolds number based on the impeller tip speed and diameter $2r_2$, while G, H and K are now the following functions of λ and x_*:

$$G(\lambda,\xi)=\int_0^{\delta^+}u^{+2}dy^+$$

$$H(\lambda,\xi)=\int_0^{\delta^+}\left(u^+\frac{\partial u^+}{\partial\xi}-\frac{\partial u^+}{\partial y^+}\int_0^{y^+}\frac{\partial u^+}{\partial\xi}dy^+\right)dy^+$$

$$K(\lambda,\xi)=\int_0^{\delta^+}\left(\frac{\partial u^+}{\partial y^+}\int_0^{y^+}u^+dy^+\right)dy^+$$

This equation can be numerically integrated along any relative streamline on the hub and the shroud and on both sides of the blade channels with the IC:

$$\delta^+(0)\simeq 10\quad\Rightarrow\quad\lambda(0)=\tfrac{1}{\kappa}\ln 10+B+6\xi$$

imposed at the origin of the BL by the lower limit of validity of the law of the wall (where it merges with the edge of the laminar sublayer). From the solution of the above equation, the nominal, displacement and momentum thickness of the boundary layers in the blade channels can be straightforwardly computed as:

$$\delta=2r_2\frac{\delta^+\lambda}{U_*\,\mathrm{Re}_D},\ \delta^*=2r_2\frac{\delta^{*+}\lambda}{U_*\,\mathrm{Re}_D}\ \text{and}\ \theta=2r_2\frac{\theta^+\lambda}{U_*\,\mathrm{Re}_D}$$

where, by definition:

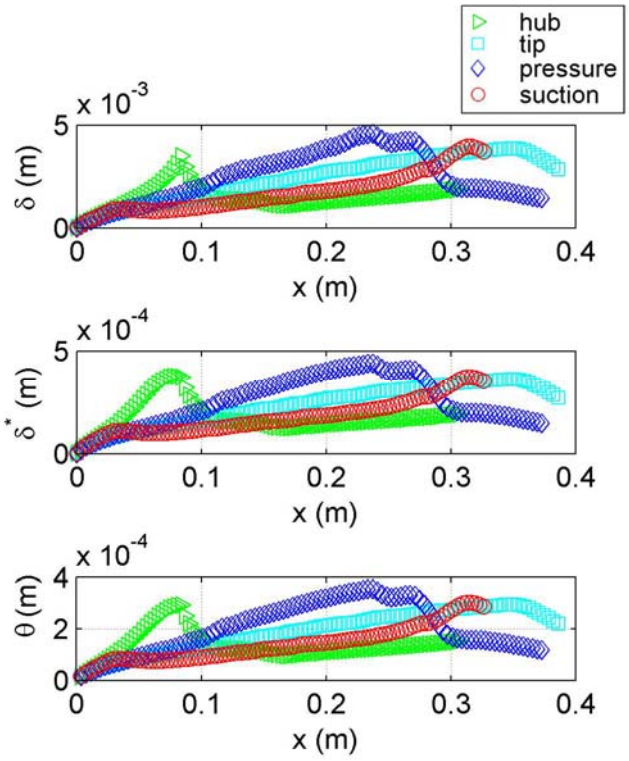

Fig.5 Boundary layer thicknesses profiles along the curvilinear streamline coordinate.

$$\delta^{*+}=\int_0^{\delta^+}\left(1-\tfrac{u^+}{U^+}\right)dy^+\ \text{and}\ \theta^+=\int_0^{\delta^+}\tfrac{u^+}{U^+}\left(1-\tfrac{u^+}{U^+}\right)dy^+$$

as required for the evaluation of impeller blockage effects, flow losses and discharge flow deviation.

At the impeller discharge, the mass averaged total pressure losses produced by perfect mixing of the azimuthal flow velocity can then be computed as:

$$\Delta p_{tM2}(z)=\frac{N}{4\pi}\rho\int_0^{2\pi/N}\left(\tilde{v}_2^2-v_S^2\right)d\vartheta'$$

where $\tilde{v}_2$ is the local azimuthal component of the vorticity correction.

DIFFUSER

The main sources of losses occurring in the diffuser are due to the friction on the walls and possibly to the sudden flow diffusion if the width of the diffuser is wider than the blade height at the impeller exit. Friction losses on the side walls can be evaluated along the nominal streamlines, consisting in a logarithmic spirals with constant φ angle with respect to the radial direction, as follows:

$$\Delta p_{tF3}=\frac{1}{2}\rho\left(u_3^2+v_3^2\right)f_D\frac{r_3\left(r_3-r_2\right)}{2b_D r_2\cos\varphi}$$

where the friction factor f_D depends on the Reynolds number based on the hydraulic diameter $D_{Hdiff}=2b_D$. Finally, total pressure losses due to the sudden variation of the flow cross-section from the impeller discharge to the diffuser can be estimated by means of:

$$\Delta p_{tD2}=\frac{1}{2}\rho\left(\bar{\boldsymbol{u}}_{b2}^2-\boldsymbol{u}_2^2\right)=\frac{1}{2}\rho\left(\bar{u}_{b2}^2-\bar{u}_2^2\frac{b_{I2}^2}{b_D^2}\right)$$

where $\bar{u}_2$ is the nominal mean absolute radial velocity at the impeller exit and $\bar{u}_{b2}$ is the corresponding velocity corrected for blockage effects.

VOLUTE

The pressure losses occurring in the volute are usually dominant with respect to the contributions from the other components of radial machines, especially at off-design conditions. Typically they comprise radial diffusion losses at the volute entrance, incidence losses at the tongue, frictional losses on the walls, azimuthal diffusion losses in the volute and mixing losses in the exhaust duct. Furthermore, the introduction of viscous effects directly affects the design of the volute because in the assumptions of the model its design only depends on the flowfield at the exit of the diffuser, which is significantly affected in particular by the flow blockage inside the impeller. As a consequence, volute geometries taking into account viscous effects are usually characterized by larger cross-sections.

The incidence losses at the entrance of the volute have been assumed equal to:

$$\Delta p_{tI3} \simeq \frac{1}{2}\rho\xi_{tLVi}\frac{1}{2\pi}\int_0^{2\pi}\left\{|\boldsymbol{u}_3|^2-\left[|\boldsymbol{u}_3|\cos\left(\varphi_3-\varphi_V\right)\right]^2\right\}d\vartheta=$$

$$=\frac{\rho\xi_{tLVi}|\boldsymbol{u}_3|^2}{4\pi}\int_0^{2\pi}\left[1-\cos^2\left(\varphi_3-\varphi_V\right)\right]d\vartheta$$

corresponding to the dissipation of a portion $\xi_{tLVi}\approx 1$ of the kinetic energy of the approach velocity component normal to the nominal orientation φ_V of the flow inside the volute.

Diffusion losses at the volute entrance have been included only when the flow enters the volute with a component of the velocity along the nominal orientation of the flow inside the volute higher that the mean flow velocity inside the volute:

$$\Delta p_{tD3}=\frac{1}{2}\rho\frac{\xi_{tLV3}}{2\pi}\int_0^{2\pi}\left[\left(|\boldsymbol{u}_3|^2\cos^2\left(\varphi_3-\varphi_V\right)-|\overline{\boldsymbol{u}}|^2\right)\right]d\vartheta$$

where $\xi_{tLV3}\simeq\xi_{tLVi}=1$ corresponds to a sudden deceleration of the incoming flow.

Moreover, if the flow velocity inside the volute decreases along the azimuthal direction, the azimuthal diffusion losses in the volute has been taken equal to:

$$\Delta p_{tD4}=\frac{1}{2}\rho\left(\overline{v}\big|_{\vartheta=0}\right)^2\xi_{tLVd}\left(1-\frac{\overline{v}\big|_{\vartheta=2\pi}}{\overline{v}\big|_{\vartheta=0}}\right)^2$$

where ξ_{tLVd} is computed in analogy with conical diffusers with equivalent divergence and fully developed turbulent flow.

Finally, as for previous machine elements, friction losses can be computed as:

$$\Delta p_{tF4}=\frac{1}{2}\rho\int_0^{2\pi}f_{vol}\frac{\overline{v}^2}{D_{Hvol}}\sqrt{1+\left(\frac{dr_C}{r_C d\vartheta}\right)^2}\,r_C d\vartheta$$

where the friction factor f_{vol} depends on the Reynolds number based on the hydraulic diameter of the volute cross-section D_{Hvol} along the azimuthal direction and the integration path follows the geometric center of the volute cross-section, at a distance r_C from the machine axis.

OVERALL EFFICIENCY

With the above results, the pumping performance becomes:

$$\Psi=\frac{\Delta p_t}{\rho\Omega^2 r_2^2}=\frac{\Delta p_{tE2}-\Delta p_{tLOSS}}{\rho\Omega^2 r_2^2}$$

where the total pressure rise computed with the Euler equation includes the effects of blockage and deviation introduced by the boundary layers in the blade channels:

$$\Delta p_{tE2}=\rho\Omega r_2\overline{v}_{2b\delta^\circ}$$

and the total pressure losses comprise all of the abovementioned sources of dissipation:

$$\Delta p_{tLOSS}=\Delta p_{tI1}+\Delta p_{tBL2}+\Delta p_{tM2}+\Delta p_{tD2}+$$
$$+\Delta p_{tF3}+\Delta p_{tI3}+\Delta p_{tD3}+\Delta p_{tD4}+\Delta p_{tF4}$$

Finally, the hydraulic efficiency of the machine has been evaluated by means of the expression:

$$\eta=\frac{\Delta p_{tE2}-\Delta p_{tLOSS}}{\Delta p_{tE2}}$$

Optimal Radial Turbopump Design

The application of the model at design conditions determines the pump head and the total pressure losses and, with these results, the values of the head coefficient, Ψ, the hydraulic efficiency, η, the specific speed, Ω_S, and radius, r_{2S}, as functions of the machine geometry, the design tip incidence angle and the properties of the working fluid. For any given working fluid and any assigned value of the impeller tip speed $\left(\Omega r_2\right)_{des}$, the hydraulic efficiency of the machine can be considered as functionally dependent on the following nondimensional parameters, i.e.:

$$\eta=\eta\left(\gamma_{T1},i_{T1},\frac{r_{T1}}{r_2},\frac{r_{H1}}{r_{T1}},\frac{z_1}{r_2},\frac{r_3}{r_2},\frac{b_D}{r_2},N\right)$$

and can therefore be maximized by means of a suitable unconstrained optimization method. If, in particular, some of the free geometric parameters of the model, say r_3, b_D and N, are fixed, then the efficiency can be considered as only function of the remaining parameters:

$$\eta=\eta\left(\gamma_{T1},i_{T1},\frac{r_{T1}}{r_2},\frac{r_{H1}}{r_{T1}},\frac{z_1}{r_2}\right)$$

and its optimization is simplified.

Usually the designer will be provided with some initial data, such as the nature of the liquid (ρ, ν), the design tip speed, $\left(\Omega r_2\right)_{des}$, the machine envelope ($r_2$, z_1), the nominal flow rate ($\dot{V}_{des}$) and the required head $\left(\Delta p_{tdes}\right)$. These input data often imply some constraints in terms of design values of either the specific speed, the head coefficient, or the specific radius. However, Ψ, Ω_S and r_{2S} are outputs of the model and cannot be directly controlled. In general, for any given choice of the free parameters of the model, the values of Ψ, Ω_S and r_{2S} will therefore be different from the design values. Hence, if, for example, a design value $\Omega_{S\,des}$ of the specific speed has to be obtained, the constraint:

$$\Omega_S=\Omega_{S\,des}$$

must be imposed to the maximization of η. An approximate but practical way to do it while still using an unconstrained optimization method consists in minimizing a figure of merit defined as the norm of the following vector:

$$\min_{\left(\gamma_{T1},i_{T1},\frac{r_{T1}}{r_2},\frac{r_{H1}}{r_{T1}},\frac{z_{st}}{r_2}\right)}\frac{1}{2}\|f\|_2^2=\frac{1}{2}\sum_{i=1}^{2}f_i^2$$

$$\text{with}\quad f_1=\left(1-\eta\right)\quad\text{and}\quad f_2=c^{\Omega_S}\left(\frac{\Omega_{S\,des}-\Omega_S}{\Omega_{S\,des}}\right)$$

where c^{Ω_S} is a suitable nondimensional weight for attaining adequate accuracy in the satisfaction of the

given constraint. The generalization to the case of multiple constraints is straightforward. In particular some constraints can be selected as target values for specific quantities not necessarily directly connected with the pumping performance. For example, Eckert and Schnell, [20], have provided the following equation for the choice of the number of impeller blades in centrifugal turbopumps:

$$N = 2\pi \cos\left[\left(\chi_1 + \chi_2\right)/2\right] \Big/ \left[C_1 \ln\left(r_2/r_1\right)\right]$$

where $C_1 = 0.35 \div 0.45$ is an empirical factor and corresponds, in first approximation, to the inverse of the solidity for a logarithmic spiral cascade. Thus for a fixed number of blades, a target for the value of the solidity can be easy defined to satisfy the previous equation. Moreover, the evaluation of the boundary layer evolution on the selected four streamlines can be used to avoid the geometrical configurations that lead to stall such as the ones in which the $d\lambda/dx_* \to \infty$.

The optimization procedure described above has been preliminarly used to design a radial turbopump satisfying the geometrical and operational inputs and constraints reported in Table 1 with no boundary layer separation at design condition.

Fig. 6 shows a rendering of the geometry of the radial turbopump obtained as a result of the optimization procedure.

The predicted pumping performance and efficiency are reported in Fig. 7, while the trajectories of the selected streamlines and the corresponding boundary layer thicknesses evolutions are respectively shown in Fig. 4 and Fig. 5.

Constraints	
$\Omega_{S\,des}$	0.8
σ_{des}	2.5
Φ_{des}	$65\%\,\Phi_{i_{T1}=0}$
Geometrical Input	
r_2	150 mm
r_3	180 mm
N	6
β_b	1°
b_{bT}	4.5 mm
Operational Input	
Ω	2000 rpm
ρ	1000 kg/m^3
ν	$6.91 \cdot 10^{-7}$ m^2/s

Tab.1 Input data for the optimization.

Conclusions

Based on the yet limited available evidence, the present theoretical model proved to represent a useful tool for preliminary design and performance analysis of radial machines.

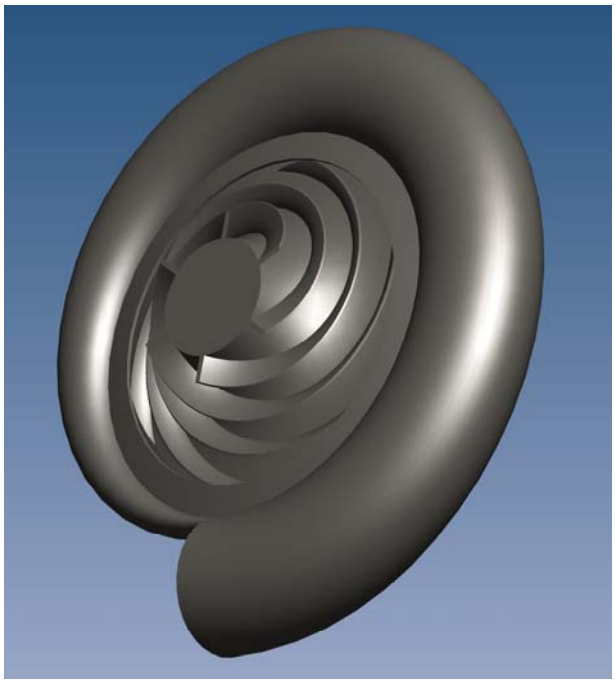

Fig.6 Rendering of the optimal radial turbopump.

More specifically, the model is able to provide quantitative indications for the geometry definition, the 3D flowfield description, the characterization and the prediction of the noncavitating pumping characteristics of radial turbopumps with complex and realistic impeller geometries.

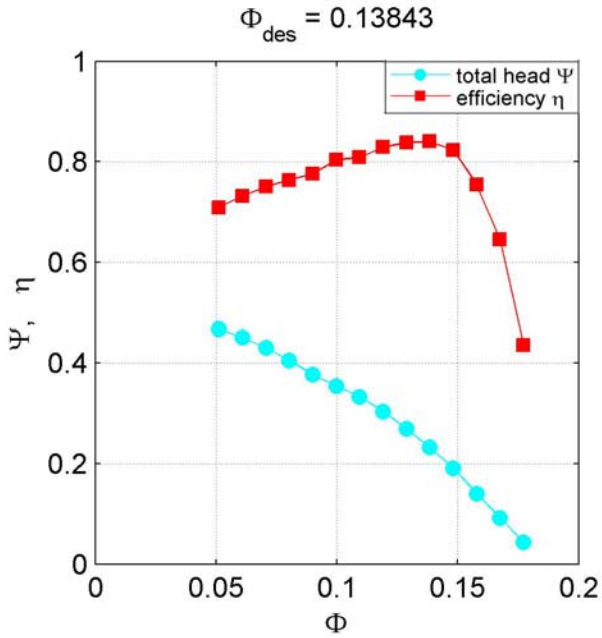

Fig.7 Optimal radial turbopump characteristic curve and efficiency.

The reduced order model presented in a previous paper, has been interfaced with the calculation of boundary layers inside the blade channels and other major forms of flow losses with the aim of developing an effective

tool for rapid parametric optimization of the machine geometry and performance. More generally, the inclusion of viscous effects in the model and its successful validation against relevant experimental data, which the authors plan to complete shortly, are expected to provide turbomachinery designers with a comprehensive interpretative framework where the main – often conflicting – aspects of radial turbomachine design and their mutual implications can be assessed, quantified and balanced in view of the attainment and optimization of the desired requirements and performance.

Aknowledgements

The present work has been supported by the European Space Agency under Contract No. 40001025856/10/NL/SFe. The authors would like to express their gratitude to Dr. Giorgio Saccoccia of ESA-ESTEC, Prof. Mariano Andrenucci and Prof. Fabrizio Paganucci of the Aerospace Department, University of Pisa, Pisa, Italy, for their constant and friendly encouragement.

References

[1] Stripling L.B. and Acosta A.J., "Cavitation in Turbopumps – Part 1", ASME Journal of Basic Engineering, Vol. 84, September 1962, pp. 326-338.

[2] Brennen, C.E., *Hydrodynamic of Pumps*, Concepts ETI, Inc. and Oxford University Press, 1994.

[3] Laskshminarayana, B., *Fluid Dynamics and Heat Transfer of Turbomachinery*, John Wiley and Sons, Inc., New York, 1985, Chaps. 1, 5.

[4] Huppertz, A., Flassig, P. M., Flassig, R. J., and Swoboda, M., 2007, "Knowledge-Based 2D Blade Design Using Multi-Objective Aerodynamic Optimization and a Neural Network", *ASME Turbo Expo 2007*, GT2007-28204.

[5] Kim, J. H., Choi, J. H., and Kim, K. Y., 2010, "Surrogate Modeling for Optimization of a Centrifugal Compressor Impeller", *International Journal of Fluid Machinery and Systems*, Vol. 3, No. 1, pp. 29-38.

[6] Choi, K. J., Kim, J. H., and Kim, K. Y., 2010, "Design Optimization of Circumferential Casing Grooves for a Transonic Axial Compressor to Enhance Stall Margin", *ASME Turbo Expo 2010*, GT2010-22396.

[7] Rai, M. M., and Madyavan, N. K., 2000, "Aerodynamic Design Using Neural Networks", *AIAA Journal*, Vol. 38, No. 1, pp. 173-182.

[8] Kim, J-H., Jin, C-H, Kim, K-Y, 2011, "Performance Improvement of a Mixed-Flow Pump by Optimization Techniques", AJK2011-06005 paper, *ASME-JSME-KSME Joint Fluids Engineering Conference*, Hamamatsu, Japan.

[9] Oh, H. W., and Kim, K. Y., 2001, "Conceptual Design Optimization of Mixed-Flow Pump Impellers Using Mean Streamline Analysis", Proceedings of the Institution of Mechanical Engineers, Part A: *Journal of Power and Energy*, Vol. 215, No. 1, pp. 133-138.

[10] Ashihara, K., and Goto, A., 2001, "Turbomachinery Blade Design using 3-D Inverse Design Method, CFD and Optimization Algorithm", *ASME Turbo Expo 2001*, 2001-GT-0358.

[11] Visser, F. C., Dijkers, R. J. H., and op de Woerd, J. G. H., 2000, "Numerical Flow-Field Analysis and Design Optimization of a High-Energy First-Stage Centrifugal Pump", *Computing and Visualization in Science*, Vol. 3, No. 1-2, pp. 103-108.

[12] Douglass, H. W., 1973, "Liquid Rocket Engine Centrifugal Flow Turbopumps," NASA SP-8109.

[13] d'Agostino, L., Torre, L., Pasini, A., Cervone, A., "On the Preliminary Design and Noncavitating Performance Prediction of Tapered Axial Inducers", *Journal of Fluids Engineering*, Vol.130, November 2008.

[14] Torre, L., Pasini, A., Cervone, A., Pace, G., Miloro, P., d'Agostino, L., "Effect of Tip Clearance on the Performance of a Three-Bladed Axial Inducer", *AIAA Journal of Propulsion and Power*, Vol. 27, No. 4, Jul-Aug 2011, pp. 890-898.

[15] Cervone, A., Torre, L., Pasini, A., d'Agostino, L., "Cavitation and Flow Instabilities in a 4-Bladed Axial Inducer Designed by Means of a Reduced Order Analytical Model", *47th AIAA/ASME/SAE/ASEE Joint Propulsion Conference*, San Diego, California, USA, August 2011.

[16] Pasini, A., Torre, L., Cervone, A., d'Agostino, L., "Characterization of the Rotordynamic Forces on Tapered Axial Inducers by Means of a Rotating Dynamometer and High-Speed Movies", *WIMRC 3rd International Cavitation Forum 2011*, University of Warwick, United Kingdom, July 2011.

[17] d'Agostino, L., Pasini, A., Valentini, D., "A Reduced Order Model for Preliminary Design and Performance Prediction of Radial Turbopumps", *47th AIAA/ASME/SAE/ASEE Joint Propulsion Conference*, San Diego, California, USA, August 2011.

[18] White, F.M, *Viscous Fluid Flow*, first edition, 1974, McGraw-Hill, Inc., New York.

[19] Mellor, G.L., 1966, *The effects of pressure gradients on turbulent flow near a smooth wall*, Journal of Fluid Mechanics, Vol. 24, Nº2, pp. 255-274.

[20] Eckert, B., and Schnell, B., 1961, *Axial and Radial Compressors* (in German), 2nd ed., Springer-Verlag, New York.